Received: 30 May 2020 | Revised: 20 November 2020 | Accepted: 11 December 2020

IET Renewable Power Generation

DOI: 10.1049/rpg2.12103

The Institution of Engineering and Technology WILEY

ORIGINAL RESEARCH PAPER

Logarithmic droop-based decentralized control of parallel converters for accurate current sharing in islanded DC microgrid applications

Monica P.[1] | **Kowsalya M.**[2] | **Josep M. Guerrero**[3]

[1] School of Electrical Engineering, Vellore Institute of Technology, Vellore, Tamilnadu 632001, India

[2] Department of Energy and Power electronics, Vellore Institute of Technology, Vellore, Tamilnadu 632014, India

[3] Department of Energy Technology, Aalborg University, Aalborg, Denmark

Correspondence
Kowsalya M., Department of Energy and Power electronics, Vellore Institute of Technology, Vellore, Tamilnadu 632014, India.
Email: mkowsalya@vit.ac.in

Abstract

Remarkable progress in distributed power generation invigorated research into DC microgrids using a controllable DC–DC converter contingent to the functionalities therein. The study explores the circulating current issue in a parallel-connected DC–DC converter and its associated current-sharing capability. Despite, the conventional droop being a promising solution with less control complexity, the current sharing is achieved at an expense of voltage drop. The prime objective of this research work is to design a control strategy that guarantees a minimized circulating current with proper current sharing for a parallel-operated DC–DC converter. This paper puts forth a dual reference-based control to alleviate the droop and load effects of the system. The primary reference is generated by considering the effect of a marginal change in the input power of the converters. The virtual resistance-based droop technique utilizes the prime reference for secondary droop reference generation. A current sharing algorithm is designed to assimilate adaptability to the scheme running under a variable line and load parameters. The comprehensive approach to the proposed control strategy has the advantages of improved current sharing and voltage regulation. A parallel DC–DC converter with the proposed control mechanism was investigated using MATLAB/Simulink and validated experimentally.

1 | INTRODUCTION

Global environmental carbon emissions along with the gradual depletion of fuel reserves has necessitated intermittent renewable energy generation in the power sector. Energy accessibility for remote communities and the democratization of power at the domestic level through the effective utilization of renewables has transformed the production of electricity [1]. The centralized paradigm of energy generation has been shifted to a decentralized form, with active distribution networks termed as distributed generation [2]. The distributed generation led to the model of microgrid that could potentially serve the power needs of pre-existing community. A simple microgrid is an integrated system of cluster of micro sources, power electronic interface (PEI), and the loads, irrespective of its connection to the utility grid [3]. Based on sizing, voltage and power level, the microgrids are classified as micro, mini, and nano grids [4]. With the liberalization of the economic markets, remarkable progress has been made in the field of microgrids during the past decade. DC microgrids were identified as an appealing choice owing to their flexible integration with renewable energy resources.

DC microgrids also hold the merits of high efficiency and better compliance with consumer electronics requirements [5]. The tapered expense of power electronics, non-existent reactive power issues, and frequency regulation problems have made DC microgrids reliable and resilient at the domestic level [6]. The demand for self-sufficiency at an affordable price in residential distribution paved the way not only for extensive research into DC–DC converters but also the development of sustainable cities and societies [7, 8]. Different architectures of low-voltage DC (LVDC) distribution systems have been discussed in the literature [9]. Figure 1 depicts the structure of autonomous low-voltage DC microgrid, which constitute source system, PEI and load system. The review of the literature in the area of

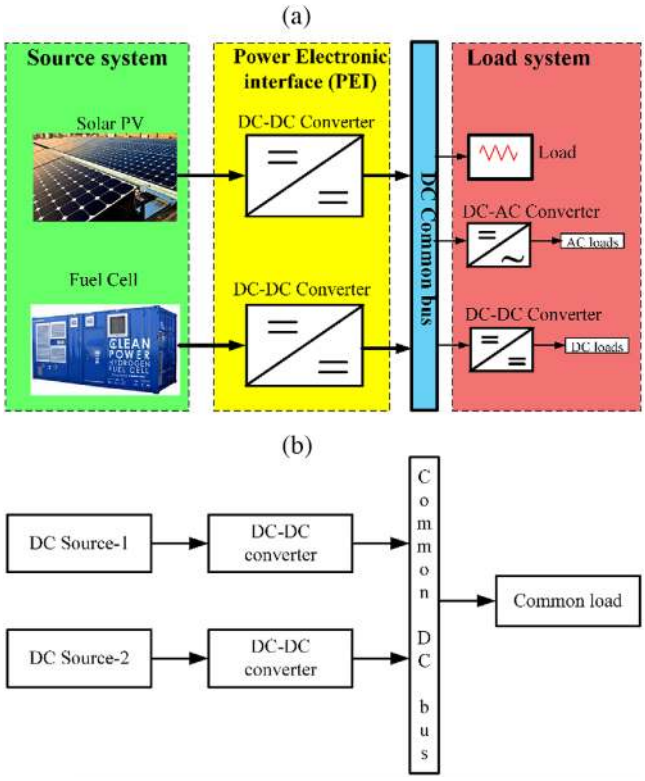

FIGURE 1 (a) Structure of autonomous LVDC microgrid. (b) Single line diagram of microgrid model for current research

DC microgrids suggests that a voltage range of 48 to 120 V in a DC system has gained significant attention because the energy distribution is efficient when compared to a 380-V DC system [10].

With diversified penetration of sources like solar, battery fuel cell, bidirectional power flow exists between the generating sources and the prosumers transforming the DC microgrid model as hybrid [11]. During the islanded operation of a DC microgrid, the parallel connection of converters in PEI is important owing to its extended power level at the output, its modularity, and easy maintenance.

These converters as power electronic interface need to cope with the uncertainties while satisfying the key power prospects. In DC microgrid, converters and inverters have low inertia which reduces stability of the system [12]. Emulating the inertia of inverters through the regulation of DC bus voltage, equips the inverter to operate as virtual synchronous generator [13, 14]. In autonomous microgrids, the virtual synchronous generator fails to regulate the DC bus voltage due to negligible grid support. Hence the DC bus voltage regulation need to be carried out at the parallel connection of the PEI especially in DC microgrids.

Hence, the current research work focuses on parallel operation of converters and its control for voltage regulation. The control of Dc microgrid includes voltage regulation of the common DC network in the parallel connection, the distribution of the load, energy storage, and monitoring [15–16].

The intermittent nature of renewable energy sources tends to cause sudden changes at the output of parallel-connected converters [17, 18]. Reasons for the flow of circulating current through the system include unequal output voltage at the common DC bus, parametric variations in terms of the line resistance, and quantitative error processing. The current research work focus on achieving accurate current sharing between the parallel converters and minimizing the circulating currents through efficient voltage regulation. Hence, simplified model of parallel DC converters feeding a common load is used for research study as shown in Figure 1(b).

Different control strategies like centralized current control, master slave technique, droop method have been proposed in the literature to address the present research problems [19–22]. The droop control strategy is widely employed since it is decentralized, wireless, and simple. The conventional droop control for power sharing is achieved at the expense of voltage deviation. The droop control method has proven to be simple and efficient method that allows for linearization of the voltage in connection with increments in the output current [23]. A generalized droop approach for current sharing proposed in [24] requires a prerequisite of line resistance parameters. Although a droop scheme based on the average value of the DC output could restore the nominal DC bus voltage, this was proven ineffective in achieving accurate load sharing during low-speed communication and its failure [25, 26]. Load sharing tends to be inaccurate owing to the effects of line impedance. Although an adaptive voltage positing system with virtual resistance was load independent and robust, it was unable to satisfy the objective of accurate load sharing when the complex line impedances were taken into account [27]. In [28], the inclination of droop resistance was varied to achieve proper power sharing, but the deviation owing to the droop was not addressed. The exchange of information between neighbouring modules of a distributed system requires a sparse communication network to tune the droop curve [29]. Most droop techniques employ a static droop value irrespective of instantaneous voltages and currents. An estimation of droop values based on a figure of merit called the droop index was proposed in [30], which needs extensive tuning of droop parameters. A compensation-based virtual impedance droop control introduced in [31, 32] regulates the power at the output based on the load applied and concentrates on power loss reduction. The reference [33] inoculates similar kind of control that compensates the DC voltage at common bus through signal injection.

An agent-based coordinated control and power management system proposed in [34, 35] also requires a communication network for load sharing. Although, the communication-based control using state estimation of microgrid through log mapping technique and least mean square algorithm was inoculated in [36, 37], the programming involved makes the process quite tedious. An approach to achieving optimal efficiency in the application of multi DC conversion systems was put forth in [38]. In [39], a control that tunes the droop curve according to the load was introduced. However, it offers poor regulation under light-load conditions owing to improper selection

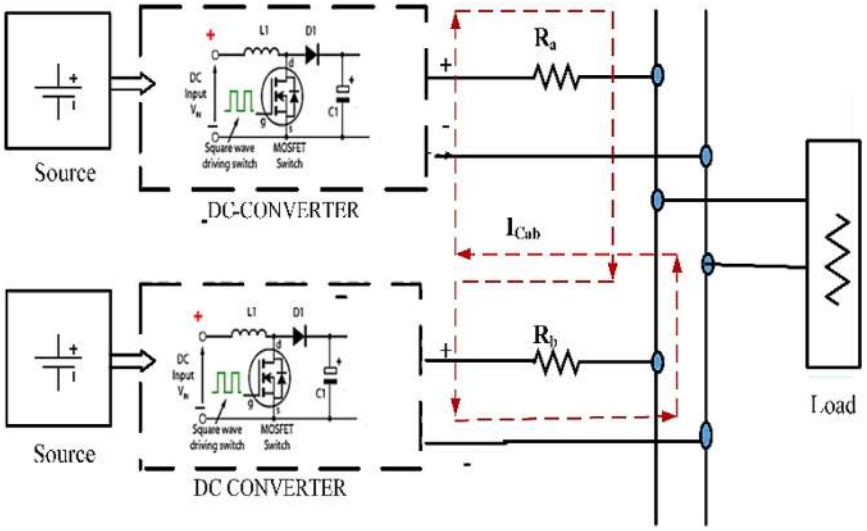

FIGURE 2 Parallel connection of DC–DC converter with circulating current flow

of the droop variable. Other studies suggested in the literature [40, 41] robust non-linear control of low-voltage DC microgrids, which still suffer from large current-sharing errors under specific load conditions. Despite the extensive research on the linear and non-linear droop control of DC microgrids, the trade-off between load sharing and voltage regulation still needs to be addressed to improve the load sharing. Reference [42] proved that the linear approximation of droop characteristics achieves high and balanced voltage regulation and load sharing.

Given these developments, this paper focuses on achieving improved current sharing with the linear approximation of a droop scheme in combination with a current-sharing algorithm in a parallel-operated DC converter.

The main contributions of the paper are as follows:

- Design and implementation of novel logarithmic droop technique to estimate linearly approximated droop coefficient for nullifying the droop effect at the source side.
- Implementing the droop compensation to transform the output voltage set point to nullify the droop effect at the load side.
- Implementing the current sharing algorithm to achieve equal current sharing among the converters and to reduce the circulating current.
- Hardware realization and detailed analysis of current sharing among the converters with the proposed control strategy, when the line resistance are equal and unequal.

The key advantage of the proposed technique, is the advantage of logarithmic function. In boundless algebraic perspective, using a logarithmic function, the marginal effect of a concerned variable that has an effect on another variable is made linear because it interprets the variable change as a percentage change. This helps to estimate the linearly approximated droop coefficients, thereby facilitating a fundamental change in the variables if any non-linearity persists.

The combination of droop control and an instantaneous current-sharing algorithm addressed in the present work improves the current-sharing capability in parallel DC converters. In addition to enhanced load sharing, the circulating current proportional to the current-sharing error is drastically minimized by means of a formulation of correction factor in the algorithm.

The paper is organized as follows. Section 2 analyses the circulating current and load sharing. Section 3 discusses the proposed logarithmic-based droop control in combination with current-sharing control. The simulation and experimental validation analysis are carried out in Section 4. Section 5 concludes the paper with a discussion of future directions.

2 | CURRENT SHARING ANALYSIS

A parallel DC–DC converter connected to a common load fed from renewable energy based controlled source is shown in Figure 2. A circulating current analysis is carried out assuming that the voltage fed from the renewable source is a constant DC supply.

V_{DC1} and V_{DC2} and I_1 and I_2 are the corresponding input voltages and currents to the converters. Let V_a and V_b be the output voltages, I_{La} and I_{Lb} be the output currents, and R_a and R_b be the line resistances of converter-A (Conv-A) and converter-B (Conv-B), respectively. V_L and I_L are the corresponding load voltage and current. Figure 3 illustrates an equivalent circuit of the parallel converter feeding the load. By applying a superposition theorem to the above circuit, currents I_{La} and I_{Lb} are obtained considering the voltage drop due to the line resistances as negligible, the equation follows as depicted below:

$$I_{La} = \frac{V_a}{(R_a + R_b \parallel R_L)} \tag{1}$$

$$I_{Lb} = \frac{V_b}{(R_b + R_a \parallel R_L)} \tag{2}$$

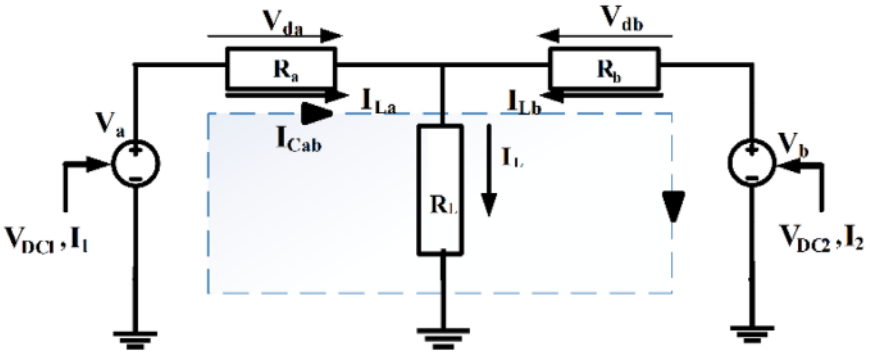

FIGURE 3 Single-line diagram of parallel DC converter

Practically, the voltage drops owing to line resistances R_a and R_b is dominant. Hence, we obtain the currents:

$$I_{La} = \frac{V_a}{(R_a + R_b||R_L)} - \frac{V_{da}}{R_a} \tag{3}$$

$$V_{da} = \left[\frac{R_a||R_L}{(R_b + R_a||R_L)}\right] V_b \tag{4}$$

Substituting Equation (4) into Equation (3), we get,

$$I_{La} = \left(\frac{V_a}{(R_a + R_b||R_L)}\right) - \left(\left[\left(\frac{R_a||R_L}{(R_b + R_a||R_L)}\right) V_b\right] \frac{1}{R_a}\right) \tag{5}$$

Similarly considering the voltage drop across R_b, the current I_{Lb} is given by:

$$I_{Lb} = \left(\frac{V_b}{(R_b + R_a||R_L)}\right) - \left(\left[\left(\frac{R_b||R_L}{(R_a + R_b||R_L)}\right) V_b\right] \frac{1}{R_b}\right) \tag{6}$$

The current sharing accuracy can be expressed as:

$$I_{Cab} = -I_{Cba} = \frac{V_a - V_b}{(R_b + R_a)} \tag{7}$$

$$= \frac{I_{La} - I_{Lb}}{2} \text{ (If } R_a == R_b) \tag{8}$$

The generalized expression for circulating current that flows from converter-a is as follows. When the line resistance connected are equal, i.e. for "$\{R_a = R_b \ldots\ldots. = R_N\}$".

$$\left\{\begin{array}{l} I_{ca} = \dfrac{I_{La} - I_{Lb}}{N} + \dfrac{I_{La} - I_{Lc}}{N} \ldots\ldots\ldots + \dfrac{I_{La} - I_{LN}}{N} \\ I_{ca} = \displaystyle\sum_{\text{Conv=b}}^{N} \frac{I_{La} - I_{LConv}}{N}; \{R_b = R_b \ldots\ldots.. = R_N\} \end{array}\right\} \tag{8a}$$

When the line resistance connected are not equal, i.e. for $\{R_a \neq R_b \ldots\ldots. \neq R_N\}$

$$I_{ca} = \frac{I_{La}R_a - I_{Lb}R_b}{(R_a + R_b)} \text{ (If} R_a \neq R_b) \tag{9}$$

$$I_{ca} == \frac{I_{La}R_a - I_{Lb}R_b}{(R_a + R_b)} + \frac{I_{La}R_a - I_{Lc}R_c}{(R_a + R_c)} \ldots.. + \frac{I_{La}R_a - I_{LN}R_N}{(R_a + R_N)} \tag{9a}$$

The expression for the circulating current suggests that currents I_{La} and I_{Lb} should be equal in order to achieve minimum circulating currents. This is possible by regulating the voltages by adjusting the equivalent resistances R_a and R_b of Conv-A and Conv-B, respectively.

2.1 | Basic concept of droop control method

Figure 3 shows the equivalent circuit of a simple microgrid configuration. The current-sharing error is minimized by the inclusion of a virtual resistance at the output of the converter. Thus, the purpose of load sharing is fulfilled. This is termed a linear droop or virtual resistance-based droop control method [28]. If R_{Da} and R_{Db} are the droop resistances, added to R_a and R_b of converter-A and converter-B, respectively, then the droop control is mathematically expressed as:

$$V_{ref,i} = V_{nom} - I_i R_{Di} \tag{10}$$

where $V_{ref,i}$, V_{nom}, R_{Di}, and I_i represent the voltage reference, nominal bus voltage, virtual droop resistance, and output current of the ith converter, where i is a and b respectively. The virtual droop resistance can be computed by assuming the voltage deviation (ΔV_i) and the maximum current rating of the converter (I_{max}). The virtual droop resistance is given by:

$$R_{Di} = \frac{\text{Voltage deviation } (\Delta V_i)}{\text{Maximum current } (I_{max,i})} \tag{11}$$

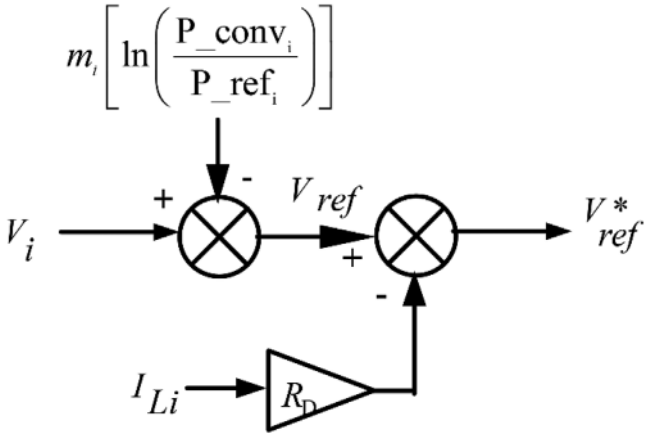

FIGURE 4 Pictorial representation of dual reference generation

The proper selection of the droop resistance minimizes the current-sharing error, which is given by:

$$\text{percentage of current sharing error} = \frac{\text{Current error}}{\text{Total current}} \times 100 = \frac{I_{La} - I_{Lb}}{I_{La} + I_{Lb}} \times 100 \tag{12}$$

3 | PROPOSED CONTROL STRATEGY

Different control strategies have been proposed in the literature, which consider only local measurements [9, 13]. The proposed control strategy in the current work combines a logarithmic droop mechanism and an instantaneous current-sharing algorithm. This control mechanism generates a dual reference based on regulation of the power and droop voltage. A correction factor is incorporated to further nullify the current-sharing error, and thus the load sharing is improved.

3.1 | Novel logarithmic droop control

The proposed logarithmic droop strategy utilizes the output power capacity of the converter and the power at the load as prime attributes in the design of the droop equation. Utilizing the nuances of the logarithmic function, the designed droop control expresses variables in percentage errors. This facilitates the linearization of the droop characteristics in case of nonlinearity. In particular, when converters are loaded with a constant power load, the system is prone to instability owing to the negative resistance. The logarithmic function incorporated in the equation stabilizes the system by identifying the exponential rise in the voltage deviation. The dual reference generation is depicted in Figure 4 and overall control diagram is depicted in Figure 5.

The difference between the rated and observed power is estimated and expressed as a percentage error through the logarithmic function. This helps to linearize and approximate the marginal effect of the power difference on the voltage, which tends to nullify the droop effect at the source side The V_{ref} reference generated can be expressed as:

$$V_{\text{ref}} = V_i - m_i \left[\ln\left(\frac{P\_\text{conv}_i}{P\_\text{ref}_i}\right)\right] \tag{13}$$

where P_conv_i is power at the ith converter; P_ref_i is the designed power capacity of ith converter, m_i is the droop coefficient.

3.2 | Droop compensation

Although the droop equation formulated in Equation (13) nullifies the droop effect owing to the source-side parameters.

Owing to the load effect, the voltage drop at the common bus is at stake. Hence, dual reference generation is put forth in this research work. The droop compensation utilizes the reference generated via the logarithmic droop as a prime reference, and the virtual resistance R_{D} is calibrated based on the novel droop method established in [28]. A new reference is generated based on the virtual resistance compensation, as shown in Equation (14).

$$V^*_{\text{ref}} = V_{\text{ref}} - I_{Li} \times R_{\text{D}i} \tag{14}$$

where V^*_{ref} is the new generated reference.

The virtual resistance R_{D} is also estimated based on a preassumed value of the error deviation method. The accuracy in determining the virtual droop resistance is indefinite. This leads to the most possible approximation of the generated reference, and the accuracy of load sharing under a step change in load is at stake. The droop resistances of converter-A and converter-B remain the same since the converters are identical. The estimated virtual resistance R_{D} of 0.13 is shown in Figure 6.

3.3 | Current-sharing algorithm

In the current scenario, to drastically nullify the current-sharing error, a correction factor (CF) is required to be incorporated in the controlling phenomenon. The correction factor depends solely on the loading factor K. This loading factor K is the ratio of the converter currents, which is proportional to their respective resistances and their equivalent loading.

$$K = \frac{I_{\text{La}}}{I_{\text{Lb}}} = \frac{V_{\text{a}}\,(R_{\text{a}} + R_{\text{D}})}{V_{\text{b}}\,(R_{\text{b}} + R_{\text{D}})} \tag{15}$$

The correction factor is also derived based on the load currents.

$$I_{\text{La}} + I_{\text{Lb}} = I_{\text{L}} \tag{16}$$

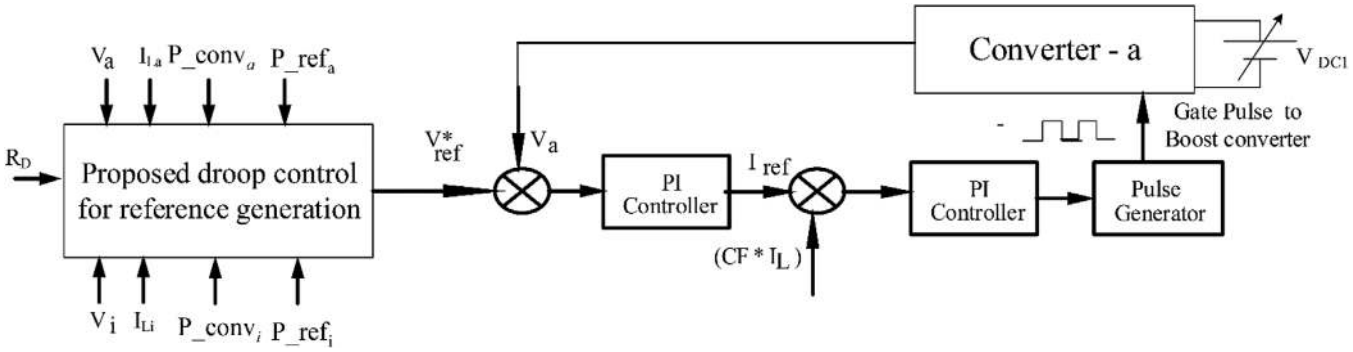

FIGURE 5 Proposed overall control loop block diagram of converter

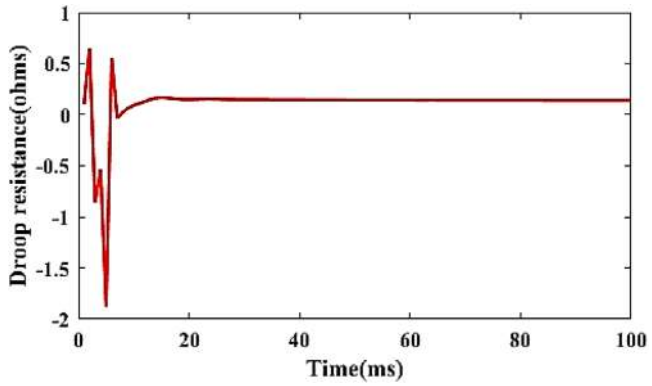

FIGURE 6 Droop resistance of converters

For accurate power sharing, the converter currents will be equal.

$$I_{\mathrm{La}} = I_{\mathrm{Lb}} \tag{17}$$

For inaccurate current sharing, the converter current equation is as follows:

$$I_{\mathrm{La}} = KI_{\mathrm{Lb}} \tag{18}$$

$$I_{\mathrm{La}} = \left[\frac{K}{K+1}\right] \times I_{\mathrm{L}} = \mathrm{CF} \times I_{\mathrm{L}} \tag{19}$$

$$I_{\mathrm{Lb}} == \left[\frac{1}{K+1}\right] \times I_{\mathrm{L}} = \mathrm{CF} \times I_{\mathrm{L}} \tag{20}$$

The deviation due to the intermittent variations at the supply side, is regulated by the algorithm. The algorithm was designed such that it also enables accurate power sharing. The flowchart in Figure 7 depicts the control algorithm that facilitates the accurate current sharing.

The flowchart in Figure 7 is represented in pseudocode as follows:

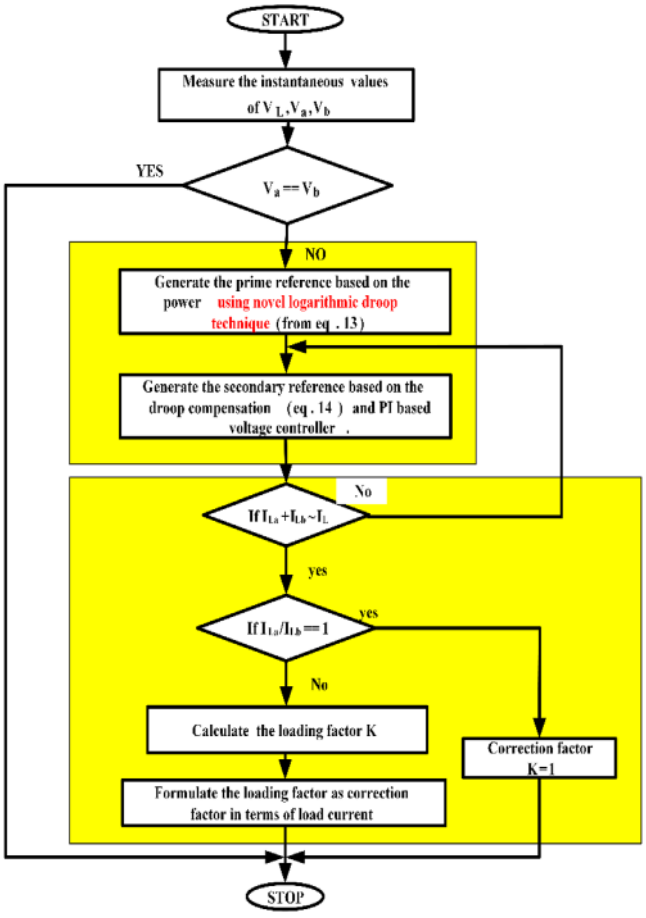

FIGURE 7 Flowchart of proposed algorithm implemented in control

1. Read the output voltage of converters and the load.
2. If the voltages of the converters are equal, then no action is required.
3. If the converters' voltages are not equal, generate the primary reference based on the proposed droop equation Equation (13).
4. Generate the secondary reference based on the virtual resistance droop represented in Equation (14), and then process the voltage error through a proportional integral (PI) controller.

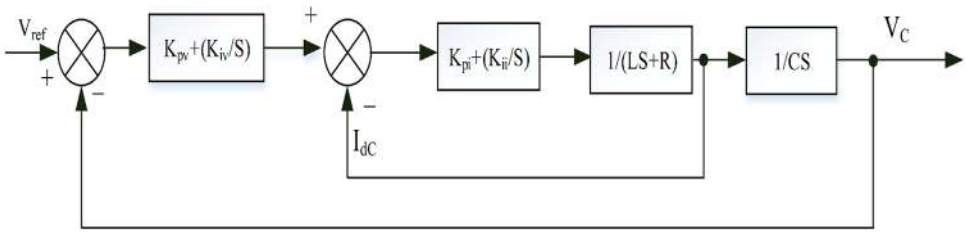

FIGURE 8 Cascade control loop of converter

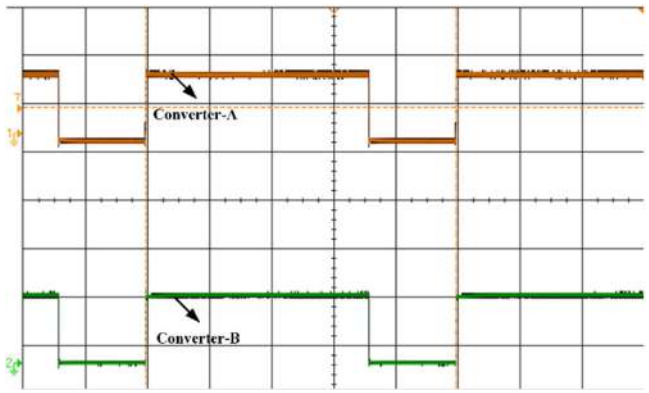

FIGURE 9 Synchronized pulse pattern of converters

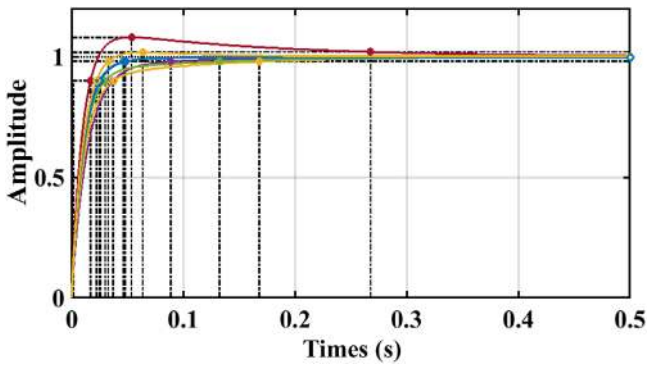

FIGURE 10 Step response of inner current loop

5. If the sum of converter currents equal to the load current, proceed to step 6, else proceed to step 4.
6. If the ratio of converter currents is unity, approximate the correction factor to 1, and stop the process.
7. Else, calculate the loading factor *K*.
8. Calculate the correction factor using the loading factor and load current and process the current error.
9. Stop the process.

3.4 | Cascade control design and stability analysis

The dual droop reference generated through the droop algorithm utilized to process the voltage and current error by means of proportional integral (PI) controller. Based on the generalized transfer function model of the boost converter, steady state frequency analysis is carried out to design the gain constants of the proportional integral controller. The control loop is as shown in Figure 8. The K_{pv}, K_{iv} are the control constants of the outer voltage loop and K_{pi}, K_{ii} are the control constants of inner current loop. Since the power stage of the converter, the reference and the control constants are the same, the control signal also remains identical. The identical control signals tend to synchronize the pulses through which the impact of the time delay is negligible. The Figure 9 depicts the synchronized pulse pattern of the parallel converters. The inner current loop utilizes the output current of the converter as feedback to process the current ratio and the outer voltage loop is used to regulate the voltage and the mismatch is overcome by the droop algorithm. The average small signal model of DC converter [43] whose closed loop transfer function model are given in Equations (21) and (22). The transfer function model of the DC converter is utilized to determine the control coefficients of Proportional-Integral control of the current and voltage control. The closed loop transfer function of inner current control (G_{ic}) is:

$$G_{ic} = \frac{\left[K_{pi} + \frac{K_{ii}}{s}\right]\left[\frac{1}{Ls+R}\right]}{1 + \left[K_{pi} + \frac{K_{ii}}{s}\right]\left[\frac{1}{Ls+R}\right]} \tag{21}$$

The closed loop transfer function model for outer voltage control (G_{vc}) is:

$$G_{vc} = \frac{\left[K_{pv} + \frac{K_{iv}}{s}\right]\left[\frac{RCs}{RCs+1}\right][G_{ic}]}{1 + \left[K_{pv} + \frac{K_{iv}}{s}\right]\left[\frac{RCS}{RCs+1}\right][G_{ic}]} \tag{22}$$

The cascade control loop is tuned using the frequency analysis plots. The step response tuning of the open loop current control is depicted in Figure 10. The rise time of the system step response is 0.0261 s (s) and the setting time of the response is 0.0465 s. The Bode analysis of the system is also carried out

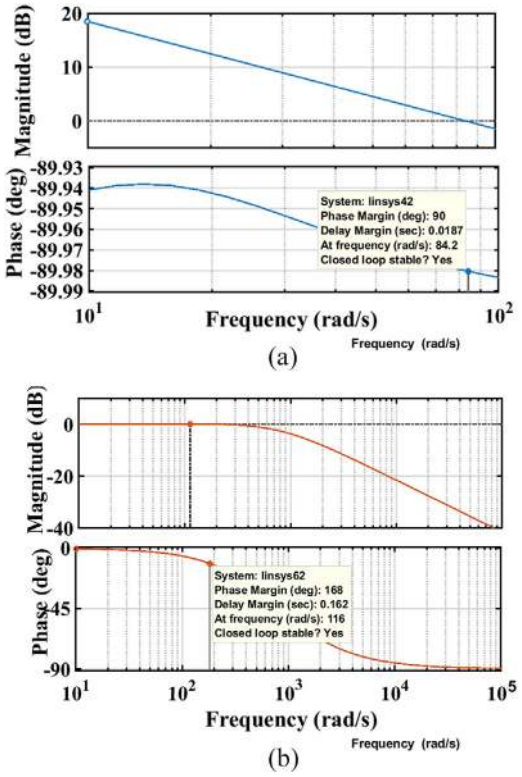

FIGURE 11 (a) Open loop Bode plot of inner current control. (b) Closed loop Bode plot of current control

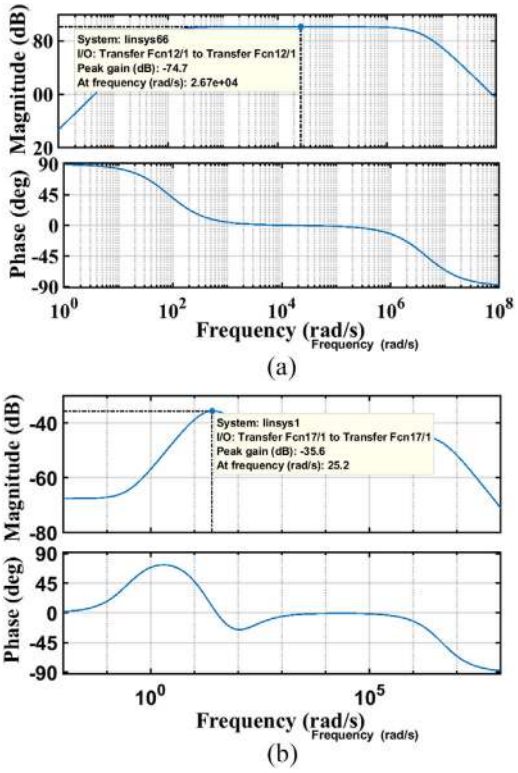

FIGURE 12 (a) Open loop Bode plot of outer voltage control. (b) Closed loop Bode plot of voltage control

to analyse the stability of the system. The uncompensated bode plot shown in Figure 11(a) represents the inductor current to input voltage transfer function which is of the first order. This indicates that the inductor current has very less impact on the output voltage and the gain coefficients are designed to improve the stability. The negative zero in the system means the zero at the left half of the S-plane do not affect the absolute stability of the system. This is much evident with the pole zero plot as shown in figure. The closed loop bode plot shown in Figure 11(b) indicates that at cross over frequency of 116 rad/s, the phase margin is 168 degrees tuned with the coefficients $K_{pi} = 0.185$ and $K_{ii} = 2.52$. Similarly, the uncompensated outer loop bode diagram is shown in Figure 12(a) and outer voltage loop is tuned with parameters $K_{pv} = 0.65$, $K_{iv} = 1.91$ and the corresponding bode plot is depicted in Figure 12(b).

The control coefficients of both the converters are designed identical since the converters are identical and voltage regulation for any change is load is completely taken care by the proposed algorithm through adjustment of reference.

The impact of communication time delay in the control algorithm is assumed less significant due to the fact that small change in delay will not affect the stability of the system [44].

Although the communication delay prospect in the proposed algorithm is not considered, the delay time based on the step response of the system is incorporated in the pulse width modulation block of the control circuit. This reduces the error between the time to error signal sampling and the time to duty update at the trial of the forthcoming switching cycle. The delay time of both the converters are designed identical which is 6.5 micro seconds, ensure the converters to operate synchronously.

TABLE 1 Parameters for simulation

	Parameter	Value
DC–DC converter	Supply voltage	VDC = (18–20) V
	Switching frequency F_s	10 kHz
	L_r	4.5 mH
	C_0	100 μF
	Line resistance	100 mΩ, 150 mΩ
Control parameters	Inner current control	$K_{pi} = 0.185$, $K_{ii} = 2.56$
	Outer voltage control	$K_{pv} = 0.65$, $K_{pi} = 1.91$

4 | SIMULATION RESULTS AND DISCUSSION

The combined logarithmic droop and instantaneous-current-algorithm control of parallel-operated DC–DC converters proposed in the research work are simulated using MATLAB/Simulink. The simulation study is carried out considering that the output voltages at the converters are different with variations in the supply voltage. The simulation parameters for the research study are depicted in Table 1.

TABLE 2 Simulated results without droop controller

Line resistance	V_a, V_b, V_L (V)	I_{La}, I_{Lb}, I_L (A)	I_{error} (A)%	I_{cir} (A)
Same	48.1, 48.24, 47.95	3.161, 1.698, 4.82	30.35	0.73
Different	48.0, 47.76, 47.57	3.139, 1.743, 4.82	28.8	0.69

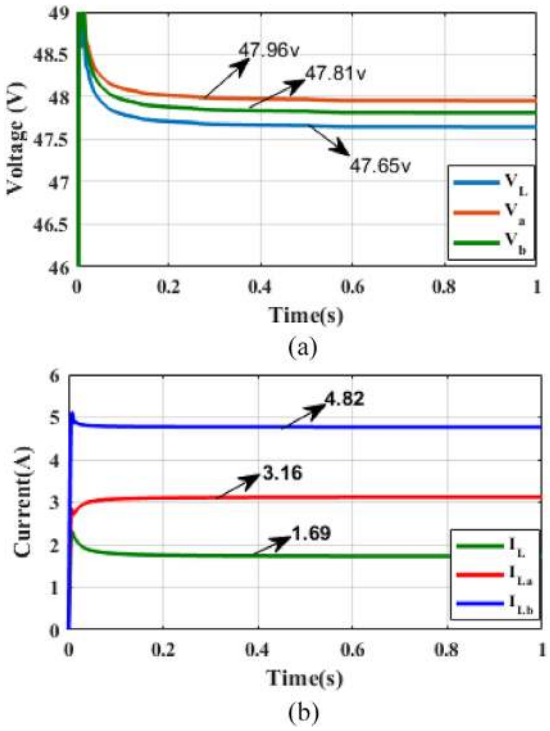

FIGURE 13 (a) Output voltages of converter-A, converter-B, and load. (b) Output currents of converter-A, converter-B, and load

4.1 | Without droop control

The parallel operation of converters without droop control is investigated with the line resistance being equal in one case and different in the other. For the same line resistance, the individual converters in parallel are connected to an output cable resistance of 100 mΩ. For different line resistances, the parallel converters are connected to resistances of 100 and 150 mΩ. The simulation results clearly illustrate improper current sharing between the parallel converters. The results are listed in Table 2.

Case (1): Same line resistance

Figure 13(a) shows the output voltages of converter-A, converter-B, and the load. Figure 13(b) depicts the output currents of converter-A, converter-B, and the load for the same line resistance of 100 mΩ connected to the output terminals of the converters.

Case (2): Different line resistances of 100 and 150 mΩ

Figure 14(a) shows the output voltages of converter-A, converter-B, and the load. Figure 14(b) depicts the output currents of converter-A, converter-B, and the load for different line resistances of 100 and 150 mΩ connected to the output terminals of the converters. Figure 14 depicts the circulating current with and without a controller.

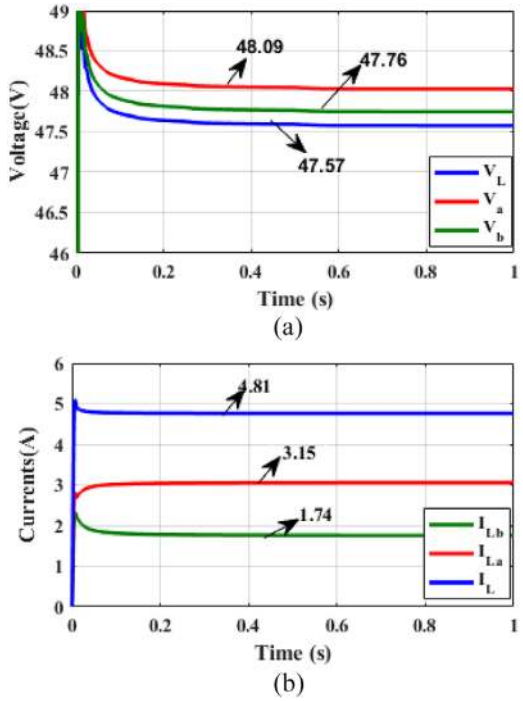

FIGURE 14 (a) Output voltages of converter-A, converter-B, and load. (b) Output currents of converter-A, converter-B, and load

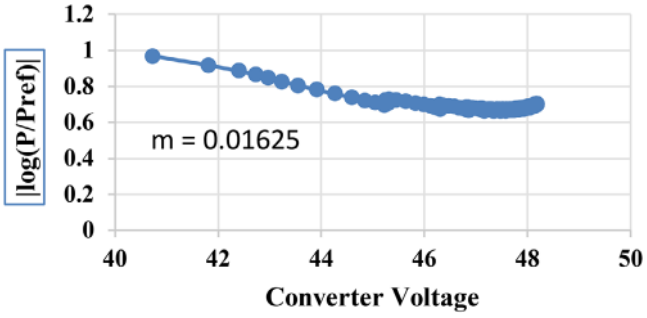

FIGURE 15 Droop coefficient estimation curve

4.2 | With proposed droop control

The proposed droop control regulates the voltage under variable supply conditions for the same cable resistance of 100 mΩ. Although the droop reference generation based on droop coefficient calculations does not nullify the current error, it helps to regulate the voltage to a satisfactory level. The droop control coefficients for converter-A and converter-B are $m_a = m_b = 0.016259$. Figure 15 illustrates the droop curve for the converter.

The droop reference generated is less adaptive. Hence, the online calculation of the droop resistance according to the change in irradiation is estimated, and a new improvised

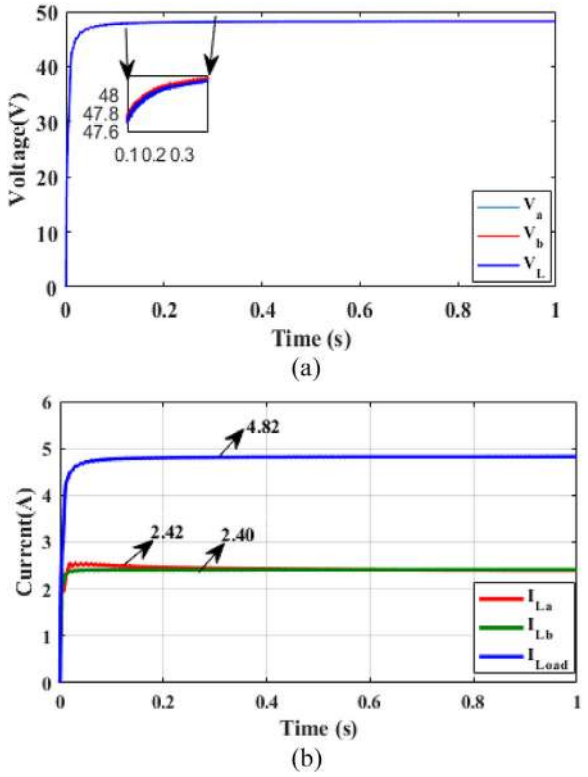

FIGURE 16 (a) Output voltages of converter-A, converter-B, and load. (b) Output currents of converter-A, converter-B, and load

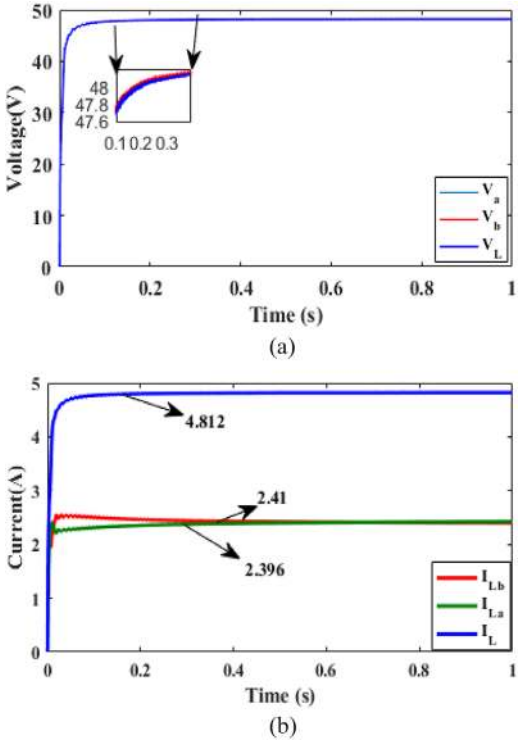

FIGURE 17 (a) Output voltages of converter-A, converter-B, and load. (b) Output currents of converter-A, converter-B, and load

reference is generated. The voltage and current errors are processed through a linear PI controller. The correction factor *K* is calibrated based on the current ratio to further assimilate the adaptability to the scheme and to succinct the converter currents for significant modifications on the either source or load side.

Case (1): Same line resistance

Figure 16(a) shows the output voltages of converter-A, converter-B, and the load. Figure 16(b) shows the output currents of converter-A, converter-B, and the load.

Case (2): Different line resistances

The simulation analysis is carried out with different line resistance. Figure 17(a) depicts the output voltage waveforms of converter-A, converter-B and load. Figure 17(b) shows the output current waveforms of converter-A, converter-B and load.

Case (3): For step change in load

The current spectrum during the change in load is depicted in Figure 18, in which the total load is increased by 25%.

The percentage of the current-sharing error for the same resistance is 0.6%, and the current-sharing error for different resistances is 1.6%. The simulation results illustrate that accurate load sharing is achieved even for a step change in the load.

Irrespective of the choice of converter and the controller, the percentage of the current-sharing error remains the prime attribute in determining the power quality through the circulating current. Table 3 depicts the better performance of the pro-

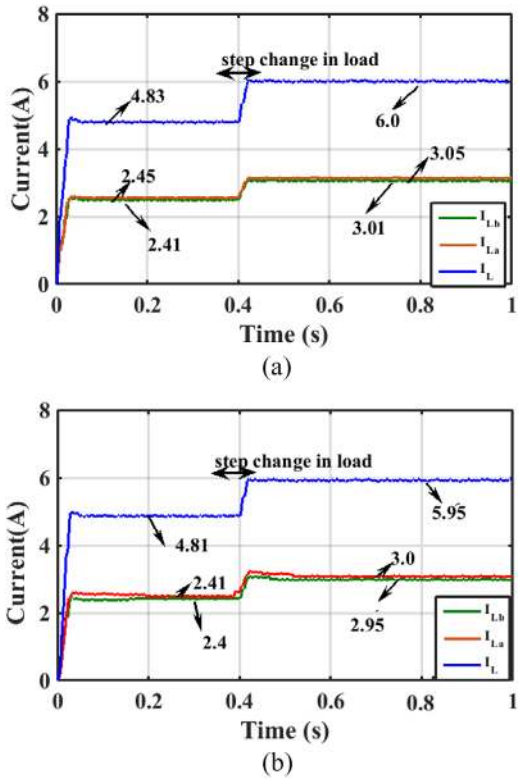

FIGURE 18 (a) Output currents of converters and load for same line resistance. (b) Output currents of converters and load for different line resistance

TABLE 3 Simulated results with proposed droop controller

Line resistance	V_a, V_b, V_L (V)	I_{La}, I_{Lb}, I_L (A)	I_{error} (A)%	I_{cir} (A)
Same	48.2, 48.2, 48.2	2.42, 2.41, 4.82	0.2	0.005
Different	48.2, 48.2, 48.19	2.41, 2.39, 4.81	0.4	0.01

posed control algorithm in terms of the current-sharing error when a simulation analysis is carried out.

5 | EXPERIMENTAL VALIDATION

To validate the proposed control strategy, a laboratory prototype of a parallel DC–DC converter is built, as shown in Figure 19. Real-time control is carried out using the real-time interface (RTI) DSPACE RTI 1202 [MicroLabBox]. Table 4 lists the specifications of the boost converter used in the experimental validation.

The regulated power supply at the supply side of the boost converter is assumed to be an irradiation variation of PV. A maximum 15% of variation is maintained between the boost converters so as to create terminal voltage difference at the input side of the converters. A constant power load is connected as a common load at the parallel connection. The hardware-in-loop simulation in DSPACE- 1202 facilitates data acquisition and the control. The model-based input-output (I/O) integration and control desk software helps evaluation during run time. The Analog input and output voltage range of the Microlab box is −10 V to +10 V and has digital I/O channels for pulse generation measurement and connection to sensors. The voltage transducer LEM-LV-25P and current transducer LEM-LA-55P shown in Figure 19 are used to sense and scale down the voltage to match the input and output range of Microlab box.

TABLE 4 Parameters for laboratory prototype

	Parameter	Value/type
DC–DC converter	Output power rating of each converters	P_o = 96 W
	Nominal output voltage of converters	V_a, V_b = 48 V
	Switching frequency F_s	10 KHz
	L_r	2.2 mH
	C_0	220 μF
	Line resistance	100,150 mΩ
	Switch	MOSFET IRF540N
Hardware platform	Dspace [Microlab box]	RTI-1202
Measurement	Voltage transducer	LEM-LV-25P
	Current transducer	LEM-LA-55P
Load	Maximum load current	(0–3) A

In a closed-loop environment, the control signal is appropriately applied to PWM block set to generate the switching pattern. Since maximum current drawn from Dspace board is 13 mA, the opto coupler-based gate driver is used to fire the MOSFET. An experimental validation is carried out for a maximum load current of 0–3 A for each converter, considering safety. Table 4 lists the parameters for the experimental laboratory prototype.

5.1 | Without droop control

A hardware-in-the-loop simulation of parallel converters connected to a common lamp load without any control is carried out. The currents at converter-A and converter-B are measured using a current clamp and are 0.95 and 1.75 A, respectively. The

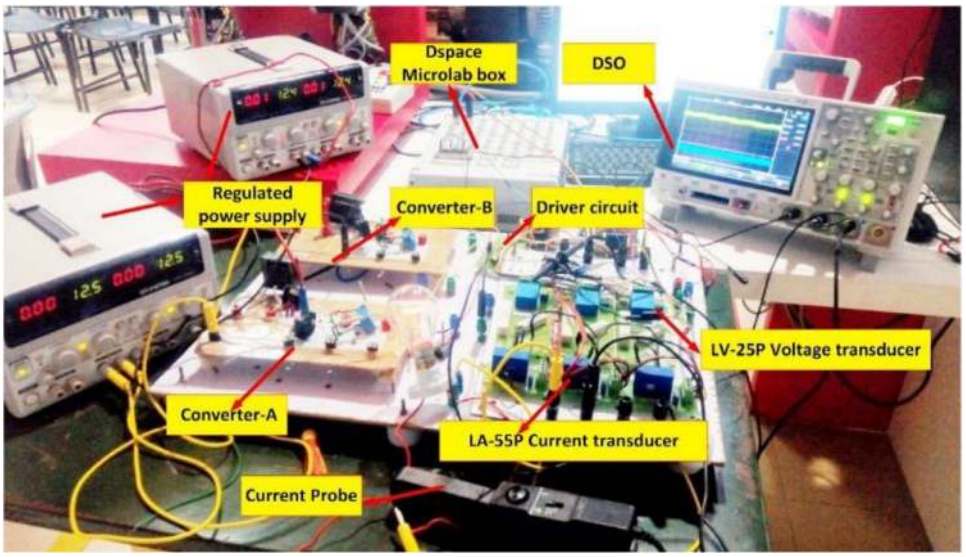

FIGURE 19 Hardware setup of DC–DC converter

TABLE 5 Experimental results without controller

Line resistance	V_a, V_b, V_L (V)	I_{La}, I_{Lb}, I_L (A)	I_{error} (A)%	I_{cir} (A)
Same	48.25, 48.1, 47.9	1.75, 0.95, 2.7	29.6	0.4

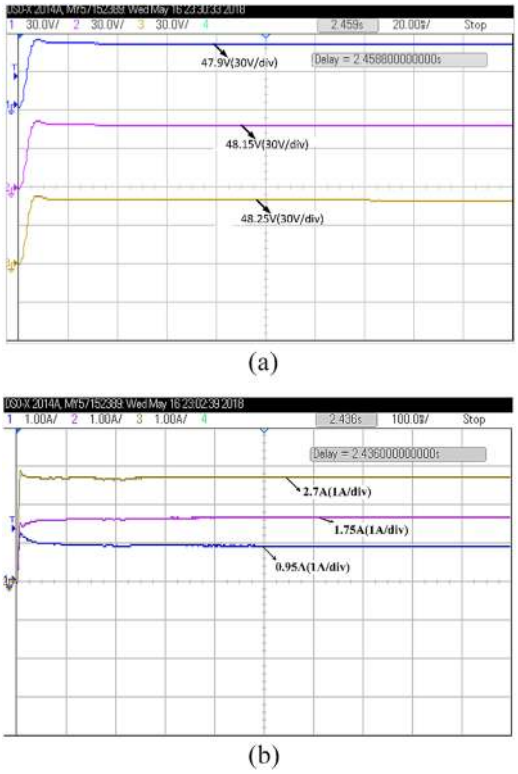

FIGURE 20 (a) Voltage waveforms without controller. (b) Current waveforms without controller

output voltages of converter-A and converter-B are measured using a differential probe and are 48 and 47.9 V, respectively. These values are listed in Table 5.

Equal load sharing can take place only when the individual converter currents are equal to 1.35 A. An experimental validation of the voltage waveform, current-sharing pattern, and circulating current waveform without a controller is shown in Figure 20(a) and Figure 20(b), respectively.

5.2 | With proposed control

The output voltage and current waveforms for the proposed control strategy are illustrated in the figures below. Irrespective of the ratings of the converters, the results clearly indicate that the proposed control strategy exhibits superior performance in terms of accurate load sharing. In the novel droop method, current sharing is achieved at the expense of a voltage drop owing to the increased droop resistance. In the proposed method, the trade-off between the output voltage and the load sharing is

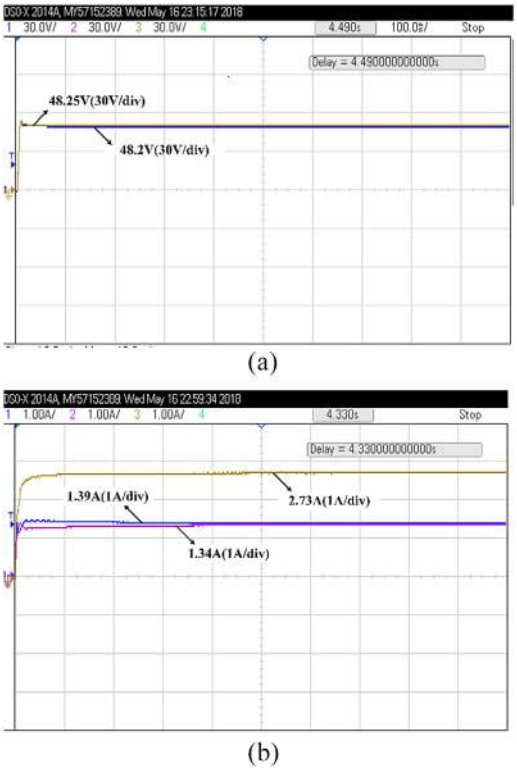

FIGURE 21 (a) Voltage waveforms with controller of same resistance. (b) Current waveforms with controller of same resistance

overcome by the dual reference generation and inclusion of the correction factor in the control algorithm.

Case (1): Same resistance

Equal line resistances of 100 mΩ each are connected to the output terminals of the converters. An experimental validation of the current-sharing capability is carried out, and the results are illustrated below. The output voltage of converter-A, converter-B, and the load are 48.25, 48.25, and 48.22 V, respectively, as shown in Figure 21(a). Although there is a slight drop in the load voltage, the correction factor in the current control loop nullifies the effect such that the current-sharing error is drastically reduced to 1.81%. The currents of converter-A, converter-B, and the load are 1.39, 1.34, and 2.73 A, respectively, as depicted in Figure 21(b).

Case (2): Different resistance

Different resistances of 100 and 150 mΩ are connected at the output terminals of converter-A and converter-B. Owing the substantial increase in the line resistance of converter-B, there exists a proportionate decrease of output current at the converter-B terminal. Despite the variation in the line resistance, the dual reference proposed in the research work balances the system's voltage and the current-sharing capability is effectively handled by the algorithm in the controller. The currents of converter-A, converter-B, and the load are 1.35, 1.25, and 2.6 A, respectively. The experimental results are shown in Figure 22(a) and Figure 22(b) and are listed in Table 6.

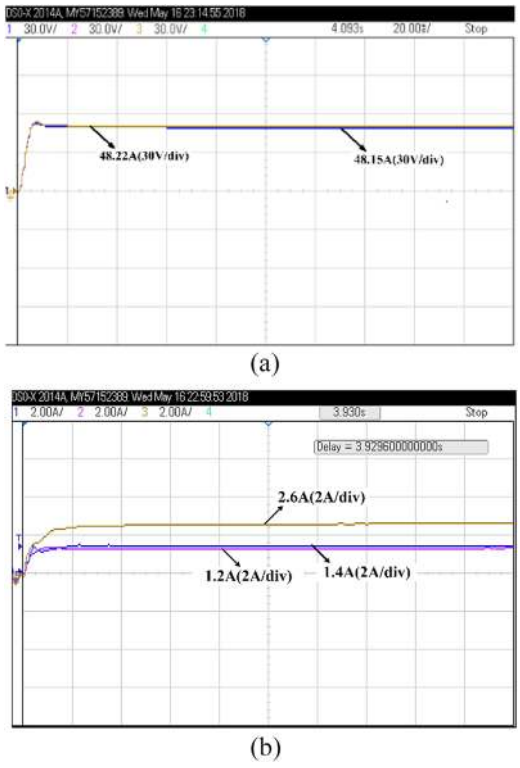

FIGURE 22 (a) Voltage waveform with controller of different line resistance. (b) Current waveform with controller of different line resistance

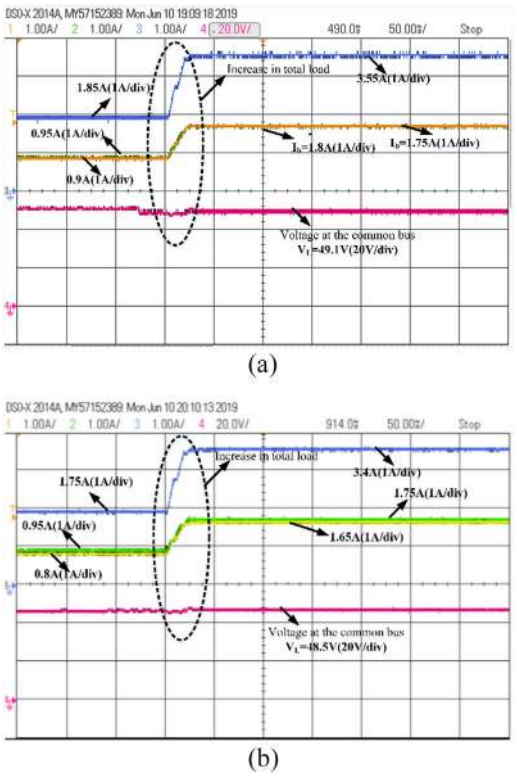

FIGURE 23 (a) Voltage and current waveform for same resistance. (b) Voltage and current waveform for different resistance

TABLE 6 Experimental results with proposed droop controller

Resistance	V_a, V_b, V_L (V)	I_{La}, I_{Lb}, I_L (A)	I_{error} (A)%	I_{cir} (A)
Same	48.25, 48.25, 48.2	1.39, 1.34, 2.73	1.81	0.025
Different	48.2, 48.2, 48.15	1.4, 1.2, 2.6	7.8	0.1

TABLE 7 Experimental results with proposed droop controller after step change in load

Resistance	V_a, V_b, V_L (V)	I_{La}, I_{Lb}, I_L (A)	I_{error} (A)%	I_{cir} (A)
Same	49.25, 49.25, 49.1	1.75, 1.8, 3.55	1.4	0.025
Different	49.2, 48.5, 48.5	1.65, 1.75, 3.4	2.9	0.05

Case (3): For step change in load

The robust control of the system can be analysed by varying the load. The total load current at the common bus is varied from 1.8 to 3.5 A, and a current-sharing analysis is carried out. Figure 23 depicts the step increase in load, voltage at the common bus, and current profile of the converters. Table 7 lists the voltage and current of the converters and load after a sudden change in load. Since the scope of the current work is limited to the control of the converter for accurate current sharing, this paper illustrates the current-sharing profile, and a robustness analysis will be carried out in future work.

Irrespective of the system rating and supply parameters, the percentage of current-sharing error in the power-sharing phenomenon remains the same analytically. From this perspective, traditional DC–DC converters exhibit 18.1% of current-sharing error [28] with the novel droop method and 2.1% with the DI method [27]. The current-sharing error is only 1.4% to 1.81% with the proposed controller. The comparative analysis of the current-sharing error put forth the superior performance of the proposed method, as shown in Figure 24. Table 8 illustrates

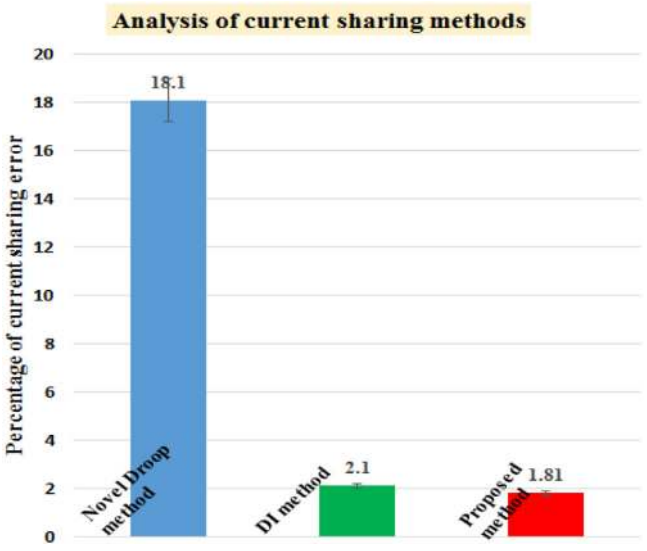

FIGURE 24 Comparative analysis of control methods

TABLE 8 Analysis of current-sharing error through different methods

Control method	Current-sharing error
Novel droop method [30]	18.1%
DI method [31]	2.1%
Proposed current-sharing method	1.8% (for same resistance)

the comparative analysis of the current sharing among different methods.

6 | CONCLUSION

The paper provides an insight into the current-sharing capability of the parallel operation of a DC–DC converter for DC microgrid applications. The scope of the current research work was limited to minimization of the circulating current and current-sharing error. In this paper, the proposed combination of the droop method and an instantaneous current-sharing algorithm drastically reduced the current-sharing error.

The proposed logarithmic droop linearizes the marginal effect of power on voltage, through which the load-sharing accuracy is improved, and the algorithm implemented in the current work offers adaptability in the control for a variable load. This feature is quite feasible when the converters are integrated with renewable energy sources such as solar PV. The proposed method is simple since the control is carried out with the measurement of local parameters.

The proposed droop control strategy proved to be efficient in terms of current sharing and minimizing the circulating current. Simulation and experimental results suggest the superior performance of the proposed droop technique for parallel DC–DC converter. Since the proposed droop scheme focuses on current sharing, the introspection of robustness analysis will be future direction of research.

NOMENCLATURE

CF	Correction factor
DC	Direct current
DG	Distributed generation
G_{ic}	Closed loop transfer function of current loop
G_{vc}	Closed loop transfer function of voltage loop
I_1	Input current to the converter-A
I_2	Input current to the converter-A
I_{ca}	Circulating current from converter-A
I_i	Output current of *i*th converter
I_{La}	Output current of converter-A
I_{Lb}	Output current of converter-B
$I_{max,i}$	Maximum current from *i*th converter
K	Loading factor
K_{ii}	Integral coefficient of current loop
K_{iv}	Integral coefficient of voltage loop
K_{pi}	Proportional coefficient of current loop
K_{pv}	Proportional coefficient of voltage loop
LVDC	Low voltage direct current
m_i	Droop coefficient of *i*th converter
N	Number of converters
P_convi	Power output of *i*th converter
P_refi	Designed power capacity of converter
PEI	Power electronic Interface
R_a	Line resistance connected to converter-A
R_b	Line resistance connected to converter-B
R_{Di}	Droop resistance of *i*th converter
R_L	Load resistance connected to common point
V_a	Output voltage of converter-A
V_b	Output voltage of converter-B
V_{da}	Drop due to line resistance
V_{DC1}	Input voltage to converter-A
V_{DC2}	Input voltage to converter-B
V_{nom}	Nominal voltage of common bus
V_{ref}*	New reference generated
$V_{ref,,i}$	Reference voltage fed to the *i*th Converter
ΔV_i	Voltage deviation of *i*th converter

REFERENCES

1. Bull, S.R.: Renewable energy today and tomorrow. Proc. IEEE 89(8), 1216–1226 (2001)
2. Dragičević, T., et al.: DC microgrids -Part I: A review of control strategies and stabilization techniques. IEEE Trans. Power Electron. 31(7), 4876–4891 (2016)
3. Monica, P., Kowsalya, M.: Control strategies of parallel operated inverters in renewable energy application: A review. Renewable Sustainable Energy Rev. 65, 885–901 (2016)
4. Mackay, L., et al.: From dc nano-and microgrids towards the universal dc distribution system-a plea to think further into the future. In: 2015 IEEE Power and Energy Society General Meeting. Denver, CO. pp. 1-5 (2015)
5. Blaabjerg, F., et al.: Recent advances in control, analysis and design of DC distribution systems and microgrids. Electr. Power Compon. Syst. 45, 1031–1039 (2017)
6. Justo, J.J., et al.: AC-microgrids versus DC-microgrids with distributed energy resources: A review. Renewable Sustainable Energy Rev. 24, 387–405 (2013)
7. Dragičević, T., et al.: DC microgrids—Part II: A review of power architectures, applications, and standardization issues. IEEE Trans. Power Electron. 31(5), 3528–3549 (2016)
8. Kumar, D., Zare, F., Ghosh, A.: DC microgrid technology: System architectures, AC grid interfaces, grounding schemes, power quality, communication networks, applications and standardizations aspects. IEEE Access. 5, 12230–12256 (2017)
9. Sasidharan, N., Singh, J.G.: A resilient DC community grid with real time ancillary services management. Sustainable Cities Soc. 28, 367–386 (2017)
10. Rodriguez-Diaz, E., et al.: An overview of low voltage DC distribution systems for residential applications. In: Consumer Electronics-Berlin (ICCE-Berlin), 2015 IEEE 5th International Conference. Berlin, pp. 318–322 (2015)
11. Patterson, M., Narciso, F.M., Arunachala, M.K.: Hybrid microgrid model based on solar photovoltaic battery fuel cell system for intermittent load applications. IEEE Trans. Energy Convers. 30(1), 359–366 (2014)
12. Cheema, K.M., Mehmood, K.: Improved virtual synchronous generator control to analyse and enhance the transient stability of microgrid. IET Renewable Power Gener. 14(4), 495–505 (2020)
13. Cheema, K.M.: A comprehensive review of virtual synchronous generator. Int. J. Power Energy Syst. 120, 106006 (2020)
14. Choopani, M., Hosseinain, S.H., Vahidi, B.: A novel comprehensive method to enhance stability of multi-VSG grids. Int. J. Power Energy Syst. 104, 502–514 (2019)

15. Bonfiglio, A., et al.: Optimal control and operation of grid-connected photovoltaic production units for voltage support in medium-voltage networks. IEEE Trans. Sustainable Energy 5(1), 254–263 (2014)
16. Vandoorn, T.L., et al.: A control strategy for islanded microgrids with dc-link voltage control. IEEE Trans. Power Delivery 26(2), 703–713 (2011)
17. Eghtedarpour, N., Farjah, E.: Control strategy for distributed integration of photovoltaic and energy storage systems in DC micro-grids. Renewable Energy 45, 96–110 (2012)
18. Yin, C., et al.: Energy management of DC microgrid based on photovoltaic combined with diesel generator and supercapacitor. Energy Convers. Manage. 132, 14–27 (2017)
19. Guangqian, D.I.N.G., et al.: Control of hybrid AC/DC microgrid under islanding operational conditions. J. Mod. Power Syst. Clean Energy 2(3), 223–232 (2014)
20. Monica, P., Kowsalya, M., Tejaswi, P.C.: Load sharing control of parallel operated single-phase inverters. Energy Procedia 117, 600–606 (2017)
21. Rajagopalan, J., et al.: Modeling and dynamic analysis of paralleled dc/dc converters with master-slave current sharing control. In Applied Power Electronics Conference and Exposition, 1996. Eleventh Annual, IEEE. Philippines, pp. 678–684 (1996)
22. Wu, T.F., Chen, Y.K., Huang, Y.H.: 3C strategy for inverters in parallel operation achieving an equal current distribution. IEEE Trans. Ind. Electron. 47(2), 273–281 (2000)
23. Guerrero, J.M., et al.: Hierarchical control of droop-controlled AC and DC microgrids—A general approach toward standardization. IEEE Trans. Ind. Electron. 58(1), 158–172 (2011)
24. Golshannavaz, S., Mortezapour, V.: A generalized droop control approach for islanded DC microgrids hosting parallel-connected DERs. Sustainable Cities Soc. 36, 237–245 (2018)
25. Lu, X., et al.: An improved droop control method for dc microgrids based on low bandwidth communication with dc bus voltage restoration and enhanced current sharing accuracy. IEEE Trans. Power Electron. 29(4), 1800–1812 (2014)
26. Tavakoli, S.D., et al.: A unified control strategy for power sharing and voltage balancing in bipolar DC microgrids. Sustainable Energy Grids Networks 11, 58–68 (2017)
27. Huang, H.H., et al. Adaptive droop resistance technique for adaptive voltage positioning in boost DC–DC converters. IEEE Trans. Power Electron. 26(7), 1920–1932 (2011)
28. Anand, S., Fernandes, B.G., Guerrero, J.M.: Distributed control to ensure proportional load sharing and improve voltage regulation in low-voltage DC microgrids. IEEE Trans. Power Electron. 28(4), 1900–1913 (2013)
29. Nasirian, V., et al.: Distributed cooperative control of DC microgrids. IEEE Trans. Power Electron. 30(4), 2288–2303 (2014)
30. Augustine, S., Mishra, M.K., Lakshminarasamma, N.: Adaptive droop control strategy for load sharing and circulating current minimization in low-voltage standalone DC microgrid. IEEE Trans. Sustainable Energy. 6(1), 132–141 (2015)
31. Kim, J.W., Choi, H.S., Cho, B.H.: A novel droop method for converter parallel operation. IEEE Trans. Power Electron. 17(1), 25–32 (2002)
32. Oureilidis, K.O., Demoulias, C.S.: A decentralized impedance-based adaptive droop method for power loss reduction in a converter-dominated islanded microgrid. Sustainable Energy Grids Networks 5, 39–49 (2016)
33. Zhang, Q., et al.: A novel autonomous current-sharing control strategy for multiple paralleled DC–DC converters in islanded DC microgrid. Energies 12(20), 3951 (2019)
34. Rahman, M.S., Oo, A.M.T.: Distributed multi-agent based coordinated power management and control strategy for microgrids with distributed energy resources. Energy Convers. Manage. 139, 20–32 (2017)
35. Meng, L., et al.: Distributed voltage unbalance compensation in islanded microgrids by using a dynamic consensus algorithm. IEEE Trans. Power Electron. 31(1), 827–838 (2015)
36. Rana, M.M., Li, L., Su, S.W.: Cyber attack protection and control of microgrids. IEEE/CAA J. Autom. Sin. 5(2), 602–609 (2017)
37. Rana, M.M.: Least mean square fourth based microgrid state estimation algorithm using the internet of things technology. PloS One 12(5), e0176099 (2017)
38. Boscaino, V., et al.: Online optimization of a multi-conversion-level DC home microgrid for system efficiency enhancement. Sustainable Cities Soc. 35, 417–429 (2017)
39. Prabhakaran, P., Goyal, Y., Agarwal, V.: Novel nonlinear droop control techniques to overcome the load sharing and voltage regulation issues in DC microgrid. IEEE Trans. Power Electron. 33(5), 4477–4487 (2017)
40. Rodríguez-Licea, M.A., et al.: Nonlinear robust control for low voltage direct-current residential microgrids with constant power loads. Energies. 11(5), 1130 (2018)
41. Khorsandi, A., et al.: Automatic droop control for a low voltage DC microgrid. IET Gener. Transm. Distrib. 10, 41–47 (2016)
42. Lin, Y., Xiao, W.: Novel piecewise linear formation of droop strategy for DC microgrid, 2019. IEEE Trans. Smart Grid. 10(6), 6747–6755 (2019)
43. Bellinaso, L.V., et al.: Cascade control with adaptive voltage controller applied to photovoltaic boost converters. IEEE Trans. Ind. Appl. 55(2), 1903–1912 (2018)
44. Shahid, M., et al.: A control methodology for load sharing system restoration in islanded DC micro grid with faulty communication links. Electronics 7(6), 90 (2018)

How to cite this article: P. M., M. K., Guerrero J.M. Logarithmic droop-based decentralized control of parallel converters for accurate current sharing in islanded DC microgrid applications. *IET Renew Power Gener.* 2021;15:1240–1254.
https://doi.org/10.1049/rpg2.12103